



*Supplement of*

**An analysis of CMAQ gas-phase dry deposition over North America through grid-scale and land-use-specific diagnostics in the context of AQMEII4**

**Christian Hogrefe et al.**

*Correspondence to:* Christian Hogrefe ([hogrefe.christian@epa.gov](mailto:hogrefe.christian@epa.gov))

The copyright of individual parts of the supplement might differ from the article licence.

# Table of Contents

Comparison of 2016 model performance results to Appel et al. (2021).....5

15 Table S1: Mapping of MODIS and NLCD LU categories to AQMEII4 LU categories (see Sections 2.3.1 and 2.3.2 for further details on different approaches between M3Dry and STAGE).....7

Table S2. Model performance statistics for all daily maximum 8-hr average O<sub>3</sub> (MDA8 O<sub>3</sub>), hourly NO<sub>x</sub> and SO<sub>2</sub>, and 24-hr average total and speciated (SO<sub>4</sub><sup>2-</sup>, NO<sub>3</sub><sup>-</sup>, organic carbon (OC) and elemental carbon (EC)) PM<sub>2.5</sub> mass samples collected at AQS monitors in 2016, including a comparison to the simulations used in Appel et al. (2021). The standard deviation over all samples is denoted as  $\sigma$  while NMB, MB, and RMSE represent the percentage normalized mean bias, mean bias, and root mean square error computed over all samples. ....8

20 Table S3. Model performance statistics for all weekly total precipitation and SO<sub>4</sub><sup>2-</sup>, NO<sub>3</sub><sup>-</sup>, and NH<sub>4</sub><sup>+</sup> wet deposition samples collected at NADP NTN monitors in 2016, including a comparison to the simulations used in Appel et al. (2021). The standard deviation over all samples is denoted as  $\sigma$  while NMB, MB, and RMSE represent the percentage normalized mean bias, mean bias, and root mean square error computed over all samples. ....9

25 Figure S1: Annual MDA8 O<sub>3</sub> and PM<sub>2.5</sub> mean biases for the M3DRY\_2016 and STAGE\_2016 base case simulations analyzed in this study this study and the corresponding “CMAQ531\_WRF411\_M3Dry\_BiDi” and “CMAQ531\_WRF411\_STAGE\_BiDi” 2016 CMAQv5.3.1 simulations analyzed in Appel et al. (2021). ....10

Figure S2. 2016 monthly mean observed and modeled concentrations at AQS sites for MDA O<sub>3</sub>, SO<sub>2</sub>, NO<sub>x</sub>, and total and speciated PM<sub>2.5</sub>. Appel\_M3DRY and Appel\_STAGE refers to the “CMAQ531\_WRF411\_M3Dry\_BiDi” and “CMAQ531\_WRF411\_STAGE\_BiDi” 2016 CMAQv5.3.1 simulations analyzed in Appel et al. (2021). ....11

30 Figure S3: Monthly mean observed and modeled precipitation and wet deposition at NADP NTN sites. Appel\_M3DRY and Appel\_STAGE refers to the “CMAQ531\_WRF411\_M3Dry\_BiDi” and “CMAQ531\_WRF411\_STAGE\_BiDi” 2016 CMAQv5.3.1 simulations analyzed in Appel et al. (2021). ....12

35 Figure S4: Impact of different WRF configuration options used in this study vs. Appel et al. (2021) on annual mean surface values of several meteorological fields, O<sub>3</sub>, and aerosol species. The maps show absolute differences calculated as M3DRY\_2016 minus M3DRY\_LTNGNO\_BASE\_2016.....13

Figure S5: Impact of different lateral boundary conditions used in this study vs. Appel et al. (2021) on annual mean surface values of several gas phase and aerosol species. The maps show absolute differences calculated as M3DRY\_2016 minus M3DRY\_HCMAQ\_2016.....14

40 Figure S6: Impact of different anthropogenic and fire emission files used in this study vs. Appel et al. (2021) on annual mean surface values of several gas phase and aerosol species. The maps show absolute differences calculated as M3DRY\_2016 minus M3DRY\_APPEL\_EMIS\_2016. “Soil” fine aerosol concentrations are estimated from simulated crustal elements as  $2.20*Al + 2.49*Si + 1.63*Ca + 2.42*Fe + 1.94*Ti$ . ....15

45 Figure S7: Impact of different lightning NO emission representation on May – September surface mixing ratios of O<sub>3</sub> and NO<sub>2</sub>, column NO<sub>2</sub>, and dry and wet deposition of total nitrogen. The maps show percentage differences calculated as  $\frac{\text{M3DRY\_LTNGNO\_BASE\_2016} - \text{M3DRY\_LTNGNO\_NLDN\_2016}}{\text{M3DRY\_LTNGNO\_BASE\_2016}}$  relative to M3DRY\_LTNGNO\_BASE\_2016.....16

Figure S8: Maps of fractional coverage of the 16 AQMEII4 LU categories (Galmarini et al., 2021) in the M3DRY\_2016 simulations using MODIS LU. As noted in Section 2.3.1, the M3Dry simulations were performed using the 20 native MODIS LU categories and the mapping to the AQMEII4 categories was performed during post-processing. None of the 20 MODIS LU categories correspond to the AQMEII4 herbaceous category.....17

50 Figure S9: Domainwide fractional coverage of the 16 AQMEII4 LU categories (Galmarini et al., 2021) in the M3DRY\_2016 and STAGE\_2016 simulations. As noted in Section 2.3.1, the M3Dry simulations were performed using the 20 native MODIS LU categories and the mapping to the AQMEII4 categories was performed during post-processing while the STAGE simulations were performed using the AQMEII4 categories. None of the 20 MODIS LU categories correspond to the AQMEII4 herbaceous category. See discussion in the text on the small differences in fractional coverage between M3DRY\_2016 and STAGE\_2016.....18

55 Figure S10. Domain average summer and winter diurnal cycles of LU-specific O<sub>3</sub> inverted stomatal resistances for M3DRY\_2016 and STAGE\_2016.....19

60 Figure S11. Domain average summer and winter diurnal cycles of LU-specific O<sub>3</sub> inverted cuticular resistances for M3DRY\_2016 and STAGE\_2016.....20

Figure S12. Domain average summer and winter diurnal cycles of LU-specific O<sub>3</sub> inverted in-canopy convective resistances for M3DRY\_2016 and STAGE\_2016.....21

65 Figure S13. Domain average summer and winter diurnal cycles of LU-specific O<sub>3</sub> inverted canopy quasi-laminar sublayer resistances for M3DRY\_2016 and STAGE\_2016. Note that in M3Dry, the quasi-laminar sublayer resistance is pathway independent while in STAGE it differs between the canopy (cuticular and stomatal) and ground (vegetated and bare soil) pathways. ....22

Figure S14. Domain average summer and winter diurnal cycles of LU-specific O<sub>3</sub> inverted ground quasi-laminar sublayer resistances for M3DRY\_2016 and STAGE\_2016. Note that in M3Dry, the quasi-laminar sublayer resistance is pathway independent while in STAGE it differs between the canopy (cuticular and stomatal) and ground (vegetated and bare soil) pathways. ....23

70 Figure S15. Domain average summer and winter diurnal cycles of LU-specific O<sub>3</sub> inverted aerodynamic resistances for M3DRY\_2016 and STAGE\_2016.....24

75 Figure S16. Left column: annual mean WRF PX grid-scale (top row) and LU-weighted sum of LU-specific  $u^*$  values for M3DRY\_2016 (second row), STAGE\_2016 (third row), and STAGE\_REF\_2016 (fourth row). Center column: absolute differences between annual mean LU-weighted sum of LU-specific and WRF PX grid-scale  $u^*$  values. Right

	columns: percentage differences between annual mean LU-weighted sum of LU-specific and WRF PX grid-scale $u *$ values.....	25
80	Figure S17. Left column: annual mean WRF PX grid-scale (top row) and LU-weighted sum of LU-specific inverted $R_a$ values for M3DRY_2016 (second row), STAGE_2016 (third row), and STAGE_REF_2016 (fourth row). Center column: absolute differences between annual mean LU-weighted sum of LU-specific and WRF PX grid-scale inverted $R_a$ values. Right columns: percentage differences between annual mean LU-weighted sum of LU-specific and WRF PX grid-scale inverted $R_a$ values. ....	26
85	Figure S18: Maps of differences in the fractional coverage of the 16 AQMEII4 LU categories (Galmarini et al., 2021) between the M3Dry simulations using WRF PX LSM configured with MODIS and NLCD LU (i.e. M3DRY_2016 and M3DRY_NLCD40_2016), respectively. Differences are shown as M3DRY_2016 -M3DRY_NLCD40_2016. As noted in Section 2.3.1, the CMAQ M3Dry calculations and post-processor estimates of LU specific and aggregated diagnostic variables were performed using native LU categories from the MODIS and NLCD schemes. Aggregation to the 16 category AQMEII4 LU scheme was performed through mapping and LU weighted averaging of equivalent categories (Table S3). None of the MODIS LU categories correspond to the AQMEII4 herbaceous category.....	27
90	References .....	28

95 **Comparison of 2016 model performance results to Appel et al. (2021)**

To provide context for the evaluation results of the CMAQ simulations performed for this study that are presented in Section 3.1, this section provides a comparison to the performance results of 2016 CMAQv5.3.1 simulations from a recent comprehensive evaluation study (Appel et al., 2021) and quantifies how differences in model configurations drive differences in model performance.

100 Table S1 and Figures S1 – S2 show model performance results for MDA8 O<sub>3</sub>, SO<sub>2</sub>, NO<sub>x</sub>, PM<sub>2.5</sub>, SO<sub>4</sub><sup>2-</sup>, NO<sub>3</sub><sup>-</sup>, OC, and EC for the M3DRY\_2016 and STAGE\_2016 base case simulations as well as the corresponding 2016 CMAQ531\_WRF411\_M3Dry\_BiDi and CMAQ531\_WRF411\_STAGE\_BiDi simulations from Appel et al. (2021). For MDA8 O<sub>3</sub>, a comparison of the AQMEII4 simulations to the Appel et al. (2021) simulations shows a positive instead of a negative bias, a larger absolute bias, a similar or lower RMSE, and a higher correlation coefficient. The AQMEII4 simulations are closer to the observations for February – July while the Appel et al. (2021) are closer for the remaining months. For NO<sub>x</sub>, the AQMEII4 simulations show slightly lower concentrations and hence a slightly more pronounced negative bias and higher RMSE compared to the Appel et al (2021) simulations but the time series indicate that all simulations deviate substantially from observations, especially during winter. For SO<sub>2</sub>, model performance is similar for all four simulations. For PM<sub>2.5</sub> mass, the AQMEII4 simulations show higher concentrations especially during summer, a positive instead of a negative bias, a larger absolute bias, a higher RMSE, and lower correlations than the corresponding Appel et al. (2021) simulations. For PM<sub>2.5</sub> species, the AQMEII4 simulations have a lower absolute bias than Appel et al. (2021) for SO<sub>4</sub><sup>2-</sup> and NO<sub>3</sub><sup>-</sup> and higher absolute bias for OC and EC. The AQMEII4 simulations also have a higher RMSE and lower correlation for all species except NO<sub>3</sub><sup>-</sup>. A comparison of the spatial patterns of MDA8 O<sub>3</sub> and PM<sub>2.5</sub> biases in Figure S1 shows that the overall higher concentrations of both pollutants in the 2016 AQMEII4 simulations resulted in a higher positive bias in the eastern U.S. compared to Appel et al. (2021) while the general underestimation in the western U.S. seen in the Appel et al. (2021) results was reduced for PM<sub>2.5</sub> and turned into a general overestimation for MDA8 O<sub>3</sub>.

120 Table S2 and Figure S3 show model performance results for weekly precipitation and wet deposition at NADP NTN monitors in 2016. Precipitation has a smaller dry bias than Appel et al. (2021) but also lower correlation coefficients and higher RMSE. This suggests that the benefit of using lightning assimilation in the WRF meteorological model predominantly is an improved representation of the temporal and spatial variability in precipitation (Heath et al., 2016). The statistics for the AQMEII4 SO<sub>4</sub><sup>2-</sup> and NO<sub>3</sub><sup>-</sup>, and NH<sub>4</sub><sup>+</sup> deposition fluxes also show lower correlations and higher RMSE compared to the Appel et al. (2021) simulations. Consistent with the negative precipitation bias, simulated wet deposition flux biases also are negative for all pollutants, though the difference between the AQMEII4 and Appel et al. (2021) simulations varies between SO<sub>4</sub><sup>2-</sup> and NO<sub>3</sub><sup>-</sup>, likely also influenced by other differences in model setup, particularly boundary conditions and lightning NO emissions. Overall, these results confirm that model performance for precipitation is a key driver for wet deposition model performance. However, despite the noticeable degradation in precipitation model performance relative to the WRF simulations described in Appel et al. (2021) that used lightning assimilation, the NMB results presented here fall within the range of retrospective long-term simulations over North America (Zhang et al., 2019).

To quantify the impacts of several differences in model inputs compared to Appel et al. (2021) on these evaluation results, Figures S4 – S7 present maps of annual mean differences between the M3DRY\_2016 base case and several of the sensitivity simulations listed in Table 1. Figure S4 shows the results of a comparison of M3DRY\_2016 against M3DRY\_LTNGNO\_BASE\_2016. The only difference between these two CMAQ simulations is the input meteorology, with M3DRY\_LTNGNO\_BASE\_2016 using the WRFv4.1.1 fields from Appel et al. summarized in Section 2.1.1. For the meteorological variables, the M3DRY\_2016 simulations show a tendency for generally lower temperatures and higher precipitation while wind speed and solar radiation show both positive and negative differences. Concentrations over land either showed small changes or decreases. Therefore, the overall higher ozone (O<sub>3</sub>) and PM<sub>2.5</sub> concentrations in M3DRY\_2016 compared to Appel et al. (2021) cannot be explained by the differences in meteorological fields. Figure S5 shows the difference in annual mean concentrations between the M3DRY\_2016 and M3DRY\_HCMAQ\_2016 simulations that differ only in their boundary conditions. Results show substantially higher MDA8 O<sub>3</sub> concentrations when using CAMS rather than H-CMAQ to generate lateral boundary conditions, with annual mean differences ranging from more than 10 ppb near the boundaries to 3-5 ppb for most of the eastern U.S. The CAMS-derived boundary conditions used in the current study also yield higher annual average PM<sub>2.5</sub> concentrations, with most of the increase caused by organic aerosols and crustal components associated with long-range transport of dust. Figure S6 shows the difference in annual mean concentrations between the M3DRY\_2010 and M3DRY\_APPEL\_EMIS\_2016 simulations that differ in their anthropogenic and wildland fire emission inputs. Use of the AQMEII4 emissions resulted in localized higher concentrations of total PM<sub>2.5</sub> compared to using the Appel et al. (2016) emissions, with partially compensating effects for different PM<sub>2.5</sub> components. Figure S7 shows the percentage difference in May - September mean surface O<sub>3</sub> and NO<sub>2</sub> concentrations, total dry and wet N deposition, and column NO<sub>2</sub> between M3DRY\_LTNGNO\_BASE\_2016 and M3DRY\_LTNGNO\_NLDN\_2016 to quantify the impact of using lightning NO emissions based on GEIA climatology in AQMEII4 rather than NLDN lightning flash data in Appel et al. (2021). The results indicate that this choice of input data has only a relatively minor impact on the surface concentrations considered in the model performance analysis but has a significant impact on modeled NO<sub>2</sub> columns which in turn impacts total nitrogen deposition, mostly through wet deposition. The noticeable impact of different datasets to represent lightning NO emissions on wet deposition of nitrogen is consistent with a recent study by Kang et al. (2022). The analysis of these sensitivity simulations indicates that the choice of lateral boundary conditions was the largest driver of differences in mean model concentrations and biases compared to the corresponding CMAQv5.3.1 simulations analyzed in Appel et al. (2021).

160

**Table S1: Mapping of MODIS and NLCD LU categories to AQMEII4 LU categories (see Sections 2.3.1 and 2.3.2 for further details on different approaches between M3Dry and STAGE)**

AQMEII4 LU Category	MODIS LU Category	NLCD LU Category
1: Water	17: Water	17: Water
2: Developed / Urban	13: Urban and Built-up	13: Urban and Built-up
		23: Developed open space
		24: Developed Low Intensity
		25: Developed Medium Intensity
		26: Developed High Intensity
3: Barren	16: Barren or Sparsely Vegetated	16: Barren or Sparsely Vegetated
		27: Barren Land
4: Evergreen needleleaf forest	1: Evergreen Needleleaf Forest	1: Evergreen Needleleaf Forest
		29: Evergreen Forest
5: Deciduous needleleaf forest	3: Deciduous Needleleaf Forest	3: Deciduous Needleleaf Forest
6: Evergreen broadleaf forest	2: Evergreen Broadleaf Forest	2: Evergreen Broadleaf Forest
7: Deciduous broadleaf forest	4: Deciduous Broadleaf Forest	4: Deciduous Broadleaf Forest
		28: Deciduous Forest
8: Mixed forest	5: Mixed Forest	5: Mixed Forest
		30: Mixed Forest
9: Shrubland	6: Closed Shrublands	6: Closed Shrublands
	7: Open Shrublands	7: Open Shrublands
		32: Shrub/Scrub
10: Herbaceous		34: Sedge/Herbaceous (not present in domain)
11: Planted/Cultivated	12: Croplands	12: Croplands
	14: Cropland-Natural Vegetation Mosaic	14: Cropland-Natural Vegetation Mosaic
		37: Pasture/Hay
		38: Cultivated Crops
12: Grassland	10: Grasslands	10: Grasslands
		33: Grassland/Herbaceous
13: Savanna	8: Woody Savanna	8: Woody Savanna
	9: Savanna	9: Savanna
14: Wetlands	11: Permanent Wetlands	11: Permanent Wetlands
		39: Woody Wetland
		40: Emergent Herbaceous Wetland
15: Tundra	18: Wooded Tundra	31: Dwarf Scrub (not present in domain)
	19: Mixed Tundra	35: Lichens (not present in domain)
	20: Barren Tundra (not present in domain)	36: Moss (not present in domain)
16: Snow and Ice	15: Snow and Ice	15: Snow and Ice
		22: Perennial Ice/snow (not present in domain)

**Table S2. Model performance statistics for all daily maximum 8-hr average O<sub>3</sub> (MDA8 O<sub>3</sub>), hourly NO<sub>x</sub> and SO<sub>2</sub>, and 24-hr average total and speciated (SO<sub>4</sub><sup>2-</sup>, NO<sub>3</sub><sup>-</sup>, organic carbon (OC) and elemental carbon (EC)) PM<sub>2.5</sub> mass samples collected at AQS monitors in 2016, including a comparison to the simulations used in Appel et al. (2021). The standard deviation over all samples is denoted as  $\sigma$  while NMB, MB, and RMSE represent the percentage normalized mean bias, mean bias, and root mean square error computed over all samples.**

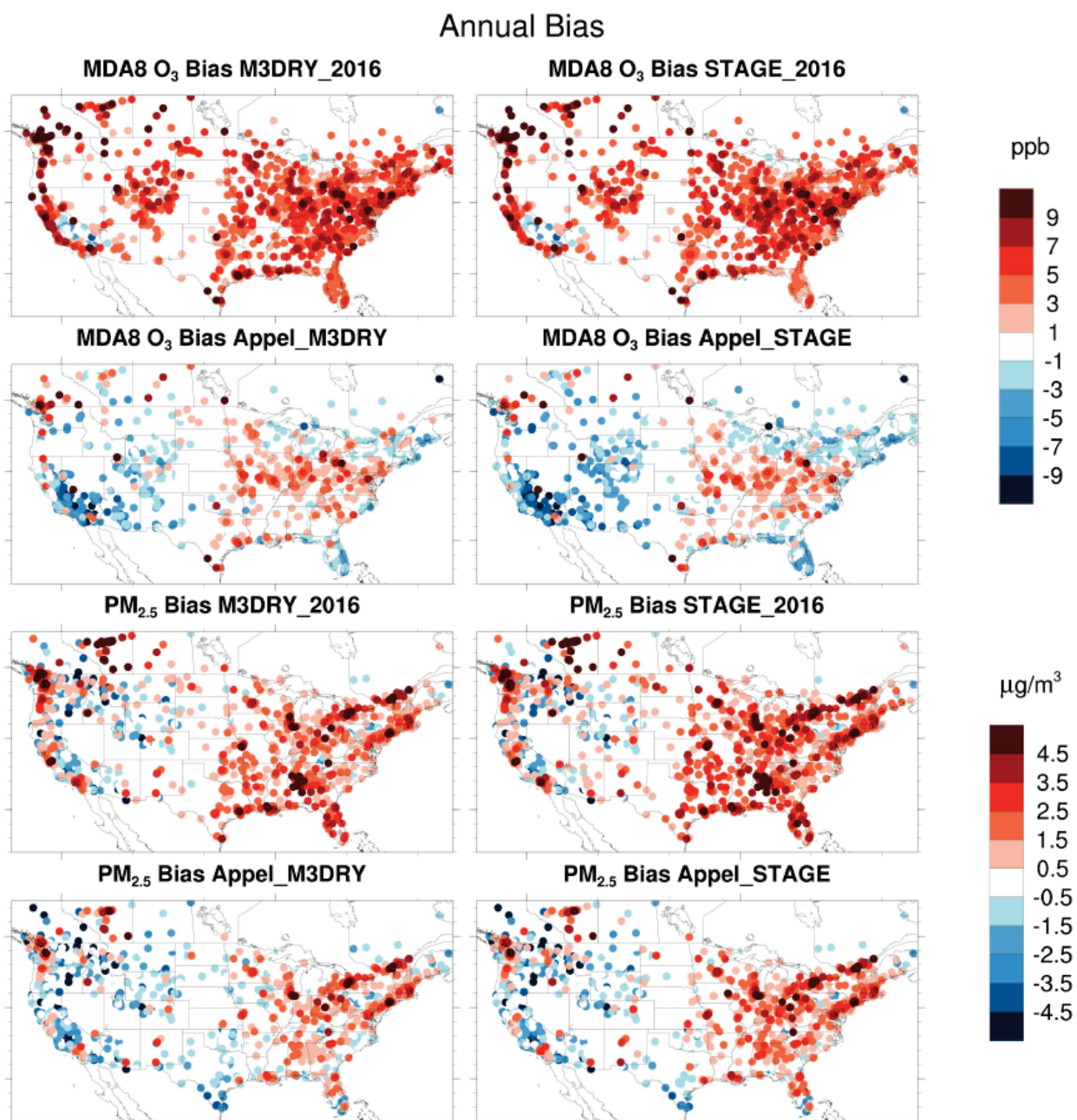
Species	Simulation	Observed Mean	Model Mean	Observed $\sigma$	Model $\sigma$	NMB	MB	RMSE	Correlation
MDA8 O <sub>3</sub> (ppb)	M3DRY BASE 2016	41.93	45.42	12.00	9.78	8.34	3.50	7.91	0.81
	M3Dry (Appel et al., 2021)		40.22		9.63	-4.06	-1.70	7.93	0.76
	STAGE BASE 2016		45.24		10.10	7.89	3.31	7.91	0.80
	STAGE (Appel et al., 2021)		39.43		10.10	-5.96	-2.50	8.50	0.74
NO <sub>x</sub> (ppb)	M3DRY BASE 2016	13.36	8.41	21.20	10.80	-37.10	-4.95	18.60	0.53
	M3Dry (Appel et al., 2021)		8.96		12.40	-33.00	-4.40	18.50	0.54
	STAGE BASE 2016		8.42		10.80	-37.00	-4.94	18.60	0.53
	STAGE (Appel et al., 2021)		9.03		12.50	-32.40	-4.33	18.40	0.54
SO <sub>2</sub> (ppb)	M3DRY BASE 2016	0.89	0.79	2.82	1.10	-11.20	-0.10	2.86	0.16
	M3Dry (Appel et al., 2021)		0.81		1.12	-8.72	-0.08	2.86	0.16
	STAGE BASE 2016		0.80		1.09	-10.10	-0.09	2.86	0.16
	STAGE (Appel et al., 2021)		0.80		1.10	-9.78	-0.09	2.86	0.16
Total PM <sub>2.5</sub> (μg/m <sup>3</sup> )	M3DRY BASE 2016	7.57	7.90	5.16	6.87	4.39	0.33	6.64	0.42
	M3Dry (Appel et al., 2021)		6.97		5.04	-7.96	-0.60	5.00	0.53
	STAGE BASE 2016		8.47		7.16	11.90	0.90	6.86	0.43
	STAGE (Appel et al., 2021)		7.47		5.32	-1.37	-0.10	5.08	0.53
SO <sub>4</sub> <sup>2-</sup> (μg/m <sup>3</sup> )	M3DRY BASE 2016	0.78	0.79	0.72	0.61	1.07	0.01	0.55	0.67
	M3Dry (Appel et al., 2021)		0.84		0.55	8.11	0.06	0.53	0.69
	STAGE BASE 2016		0.83		0.64	6.60	0.05	0.56	0.67
	STAGE (Appel et al., 2021)		0.87		0.56	11.90	0.09	0.53	0.69
NO <sub>3</sub> <sup>-</sup> (μg/m <sup>3</sup> )	M3DRY BASE 2016	0.59	0.46	1.24	0.97	-21.30	-0.13	1.00	0.62
	M3Dry (Appel et al., 2021)		0.41		0.87	-31.00	-0.18	1.01	0.60
	STAGE BASE 2016		0.53		1.07	-8.89	-0.05	1.00	0.63
	STAGE (Appel et al., 2021)		0.51		1.00	-13.30	-0.08	1.00	0.62
OC (μg/m <sup>3</sup> )	M3DRY BASE 2016	1.31	1.83	1.56	1.68	39.90	0.52	1.71	0.50
	M3Dry (Appel et al., 2021)		1.43		1.57	9.22	0.12	1.51	0.54
	STAGE BASE 2016		1.98		1.77	51.90	0.68	1.80	0.51
	STAGE (Appel et al., 2021)		1.54		1.67	18.30	0.24	1.57	0.54
EC (μg/m <sup>3</sup> )	M3DRY BASE 2016	0.31	0.39	0.40	0.46	23.50	0.07	0.40	0.61
	M3Dry (Appel et al., 2021)		0.32		0.41	1.20	0.00	0.33	0.68
	STAGE BASE 2016		0.39		0.47	25.20	0.08	0.40	0.61
	STAGE (Appel et al., 2021)		0.32		0.41	2.83	0.01	0.33	0.68

175

**Table S3. Model performance statistics for all weekly total precipitation and SO<sub>4</sub><sup>2-</sup>, NO<sub>3</sub><sup>-</sup>, and NH<sub>4</sub><sup>+</sup> wet deposition samples collected at NADP NTN monitors in 2016, including a comparison to the simulations used in Appel et al. (2021). The standard deviation over all samples is denoted as  $\sigma$  while NMB, MB, and RMSE represent the percentage normalized mean bias, mean bias, and root mean square error computed over all samples.**

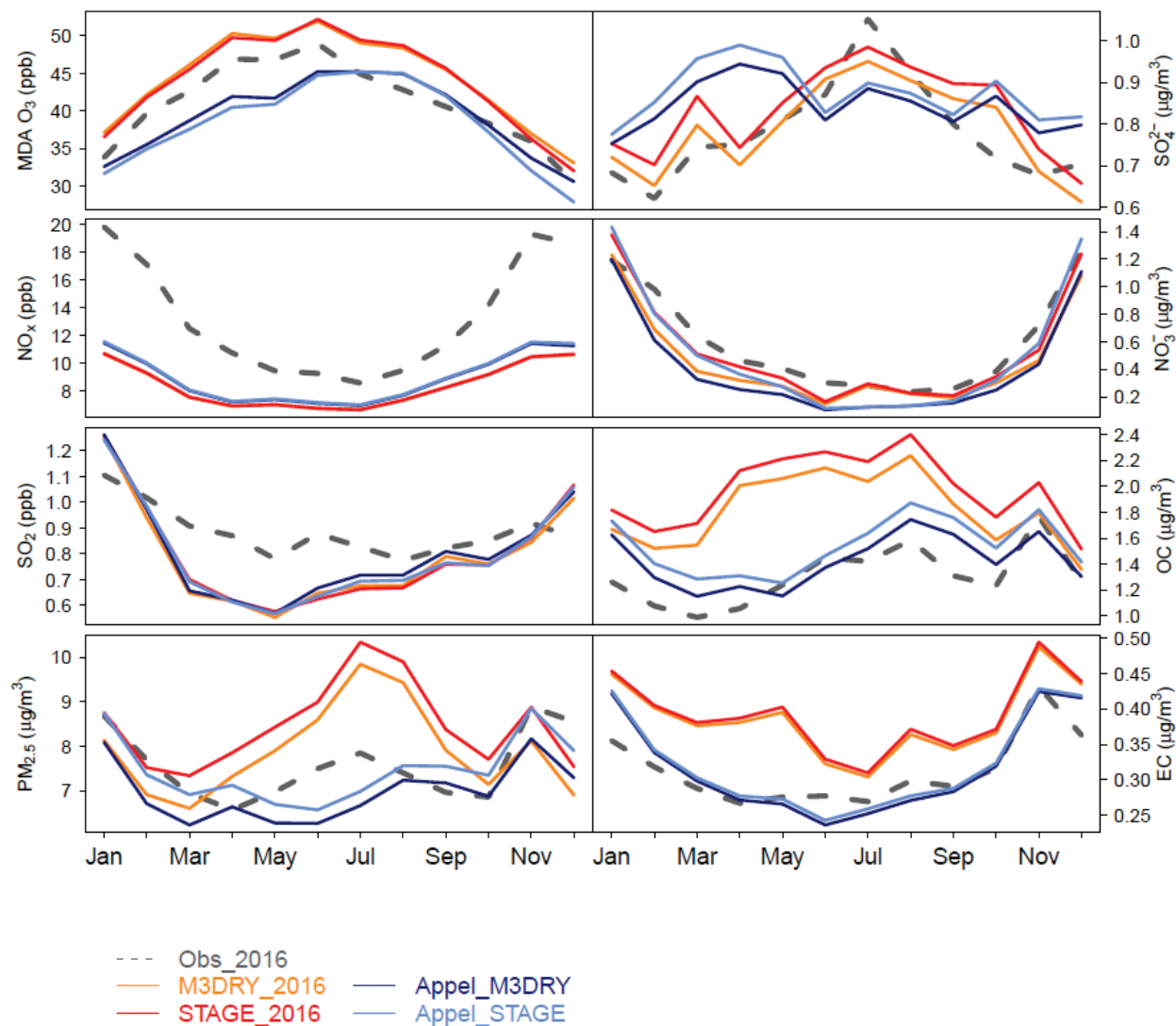
Species	Simulation	Observed Mean	Model Mean	Observed $\sigma$	Model $\sigma$	NMB	MB	RMSE	Correlation
Precipitation (mm)	M3DRY BASE 2016	19.89	19.52	26.40	25.00	-1.84	-0.37	19.30	0.72
	M3Dry (Appel et al., 2021)		18.11		23.80	-8.94	-1.78	17.00	0.78
	STAGE BASE 2016		19.52		25.00	-1.84	-0.37	19.30	0.72
	STAGE (Appel et al., 2021)		18.11		23.80	-8.94	-1.78	17.00	0.78
SO <sub>4</sub> <sup>2-</sup> (kg/ha)	M3DRY BASE 2016	0.088	0.078	0.130	0.130	-11.600	-0.010	0.115	0.61
	M3Dry (Appel et al., 2021)		0.071		0.101	-18.900	-0.017	0.097	0.68
	STAGE BASE 2016		0.080		0.131	-9.050	-0.008	0.115	0.61
	STAGE (Appel et al., 2021)		0.070		0.096	-20.700	-0.018	0.096	0.69
NO <sub>3</sub> <sup>-</sup> (kg/ha)	M3DRY BASE 2016	0.118	0.101	0.150	0.125	-14.200	-0.017	0.126	0.6
	M3Dry (Appel et al., 2021)		0.109		0.143	-7.580	-0.009	0.115	0.69
	STAGE BASE 2016		0.103		0.127	-12.700	-0.015	0.127	0.6
	STAGE (Appel et al., 2021)		0.110		0.144	-6.490	-0.008	0.115	0.7
NH <sub>4</sub> <sup>+</sup> (kg/ha)	M3DRY BASE 2016	0.055	0.027	0.085	0.046	-50.200	-0.027	0.079	0.49
	M3Dry (Appel et al., 2021)		0.029		0.047	-47.700	-0.026	0.074	0.58
	STAGE BASE 2016		0.031		0.051	-43.000	-0.024	0.076	0.52
	STAGE (Appel et al., 2021)		0.033		0.051	-39.800	-0.022	0.070	0.62

180



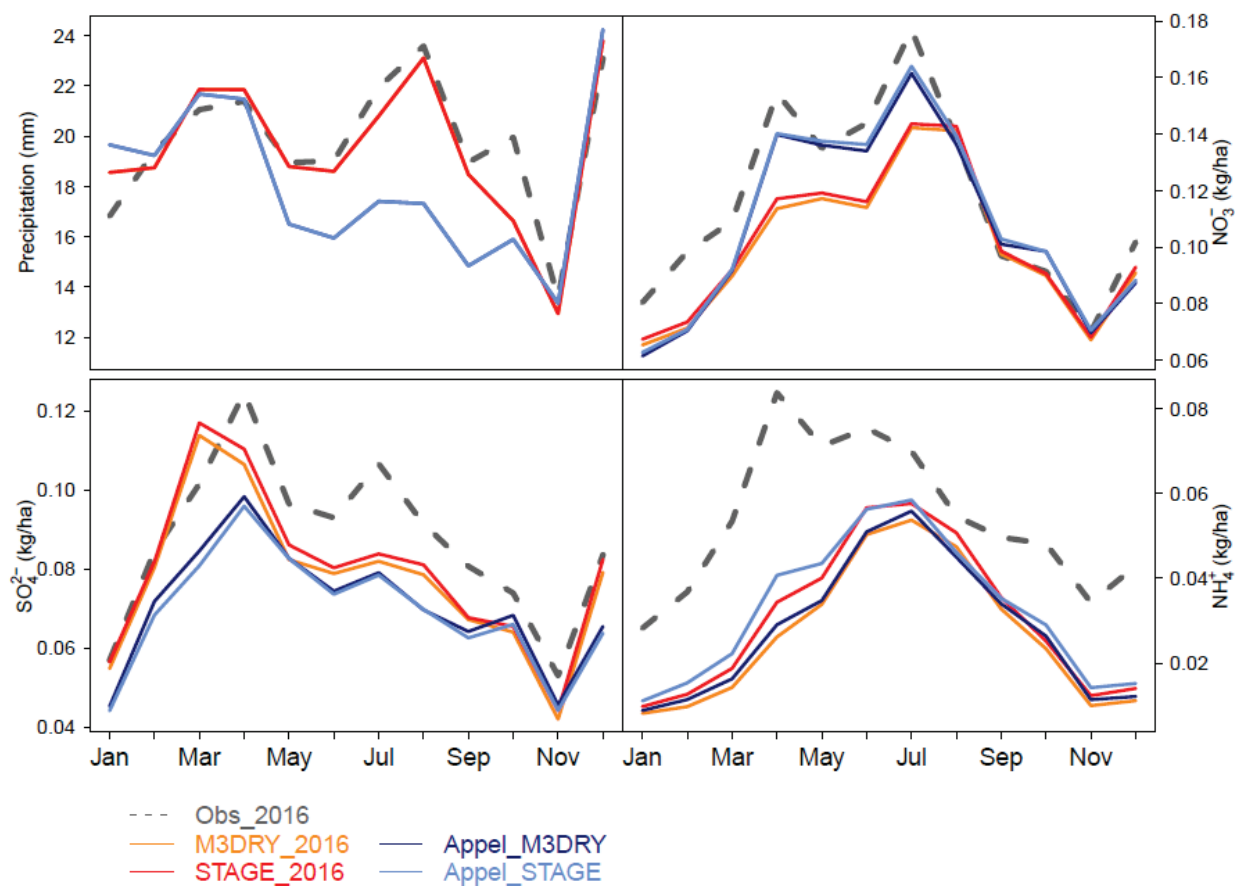
185 **Figure S1: Annual MDA8 O<sub>3</sub> and PM<sub>2.5</sub> mean biases for the M3DRY\_2016 and STAGE\_2016 base case simulations analyzed in this study this study and the corresponding “CMAQ531\_WRF411\_M3Dry\_BiDi” and “CMAQ531\_WRF411\_STAGE\_BiDi” 2016 CMAQv5.3.1 simulations analyzed in Appel et al. (2021).**

### 2016 Monthly Mean

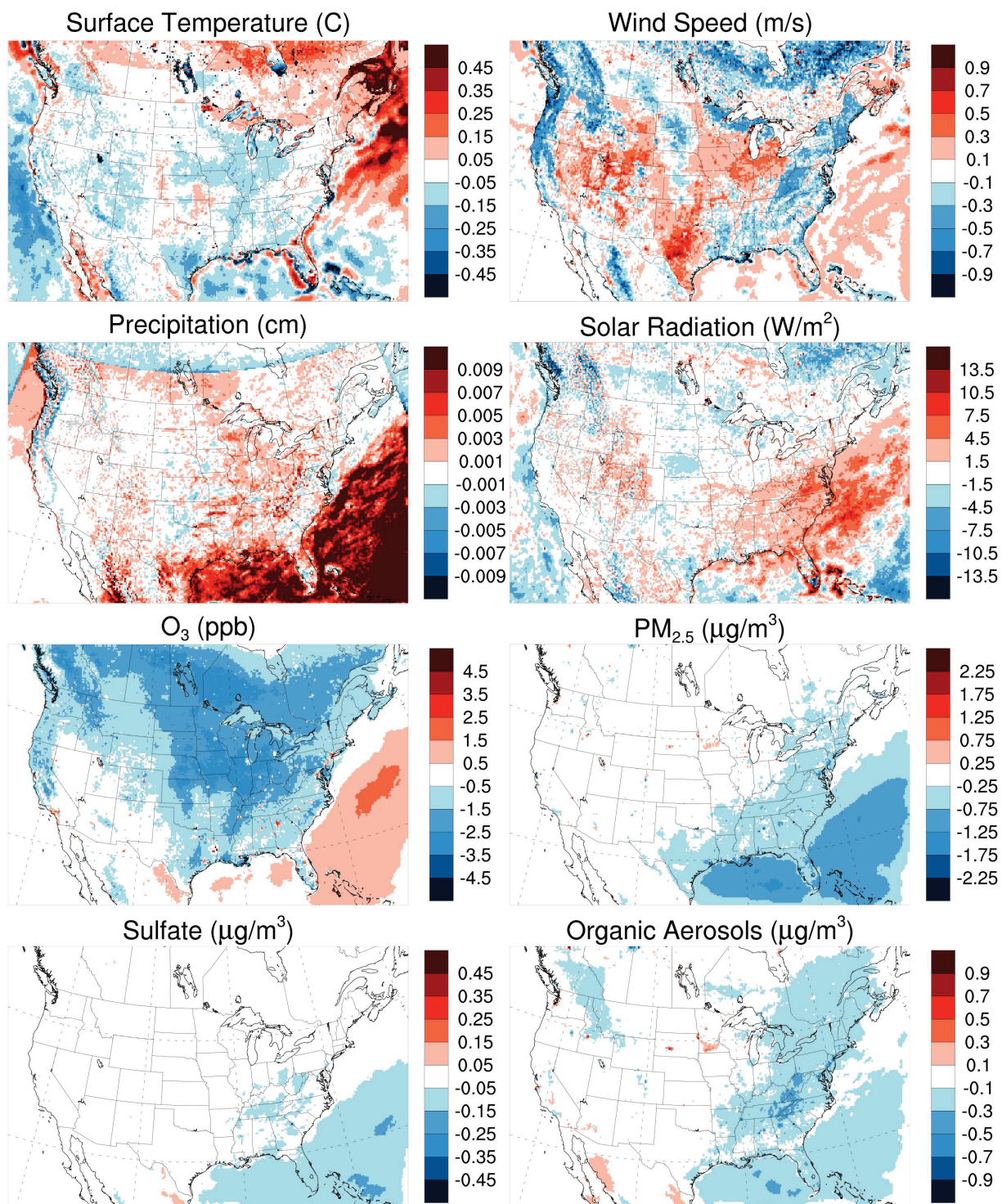


190 **Figure S2. 2016 monthly mean observed and modeled concentrations at AQS sites for MDA O<sub>3</sub>, SO<sub>2</sub>, NO<sub>x</sub>, and total and speciated PM<sub>2.5</sub>. Appel\_M3DRY and Appel\_STAGE refers to the “CMAQ531\_WRF411\_M3Dry\_BiDi” and “CMAQ531\_WRF411\_STAGE\_BiDi” 2016 CMAQv5.3.1 simulations analyzed in Appel et al. (2021).**

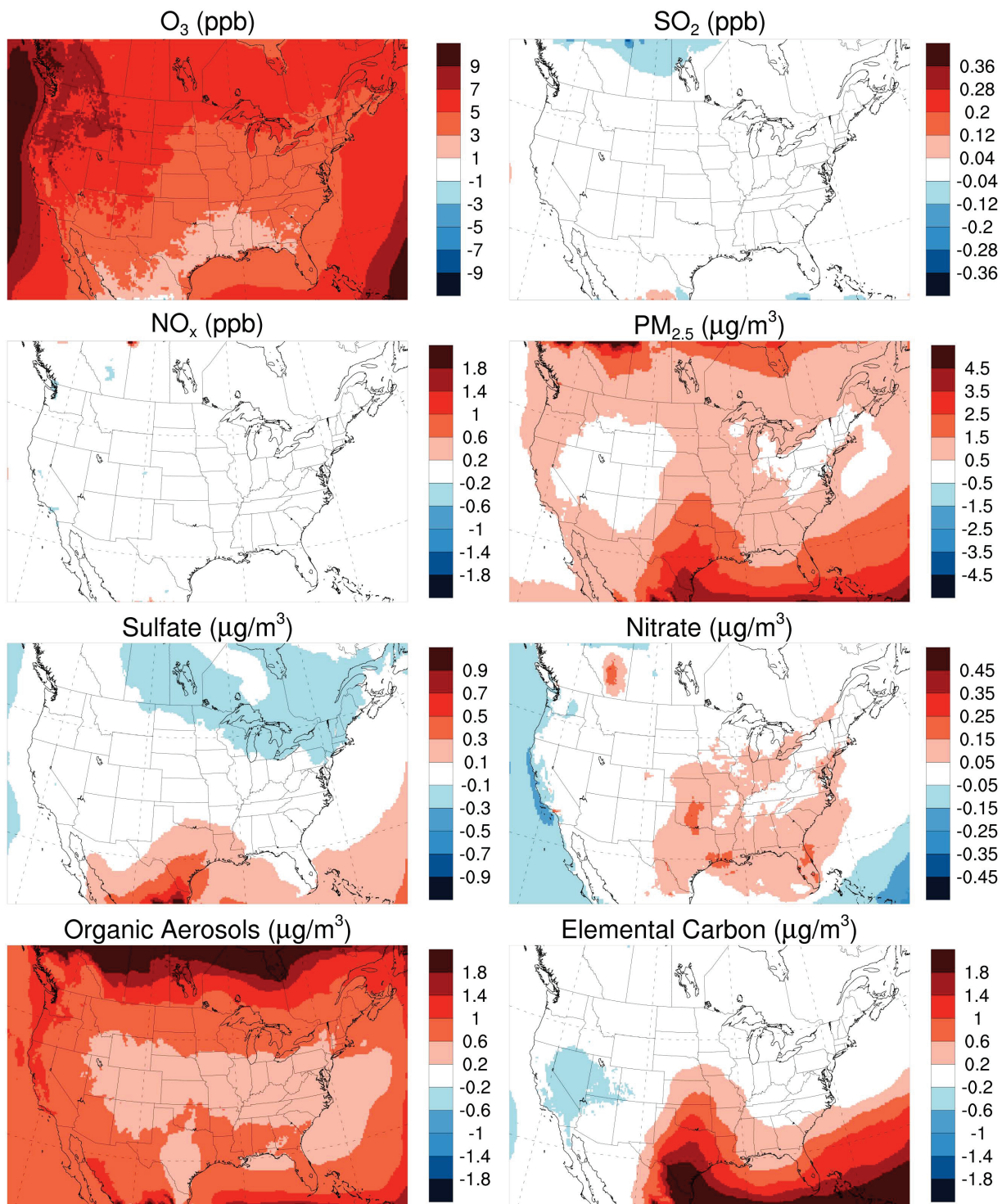
### 2016 Monthly Means of Weekly Totals



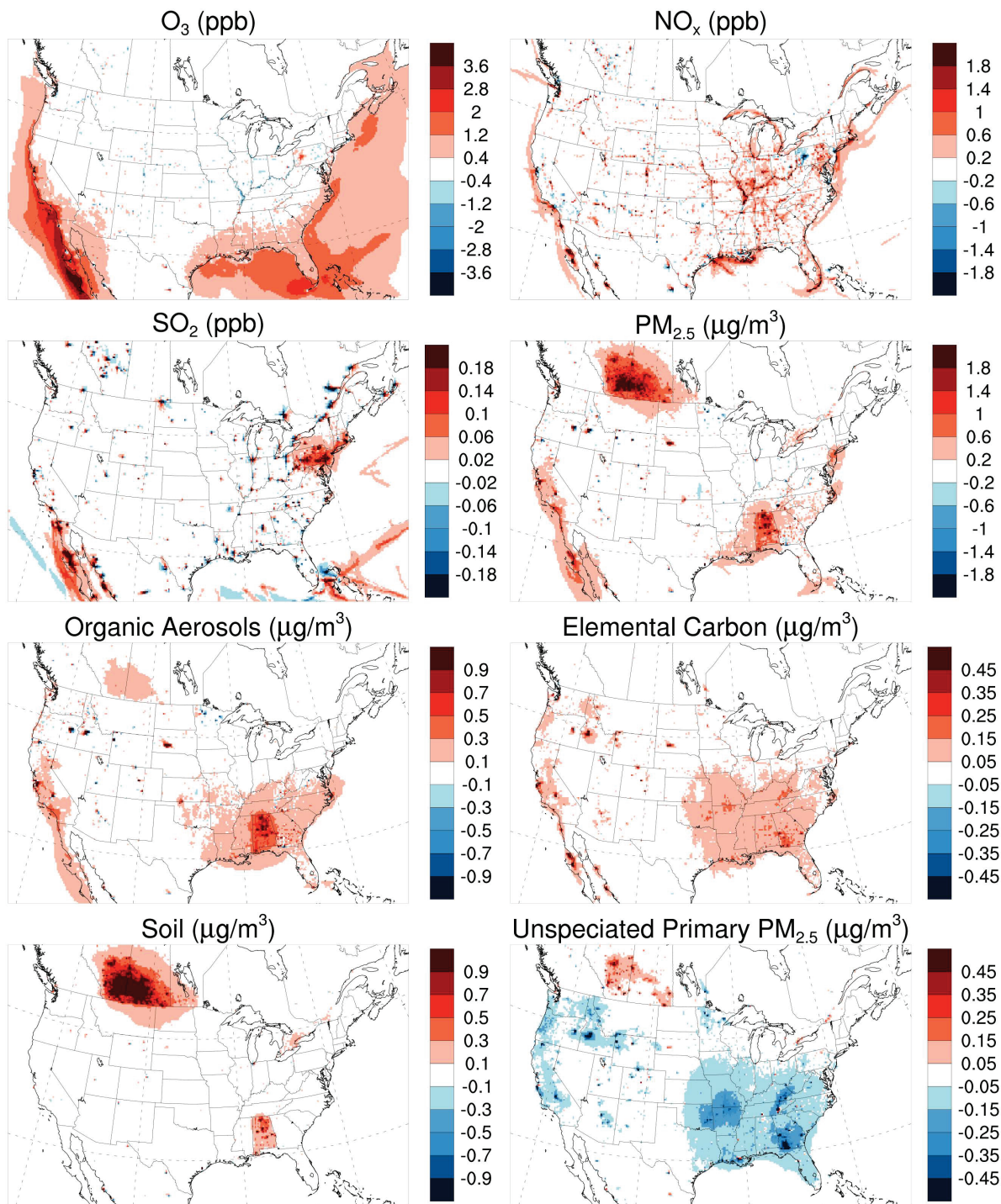
195 **Figure S3: Monthly mean observed and modeled precipitation and wet deposition at NADP NTN sites. Appel\_M3DRY and Appel\_STAGE refers to the “CMAQ531\_WRF411\_M3Dry\_BiDi” and “CMAQ531\_WRF411\_STAGE\_BiDi” 2016 CMAQv5.3.1 simulations analyzed in Appel et al. (2021).**



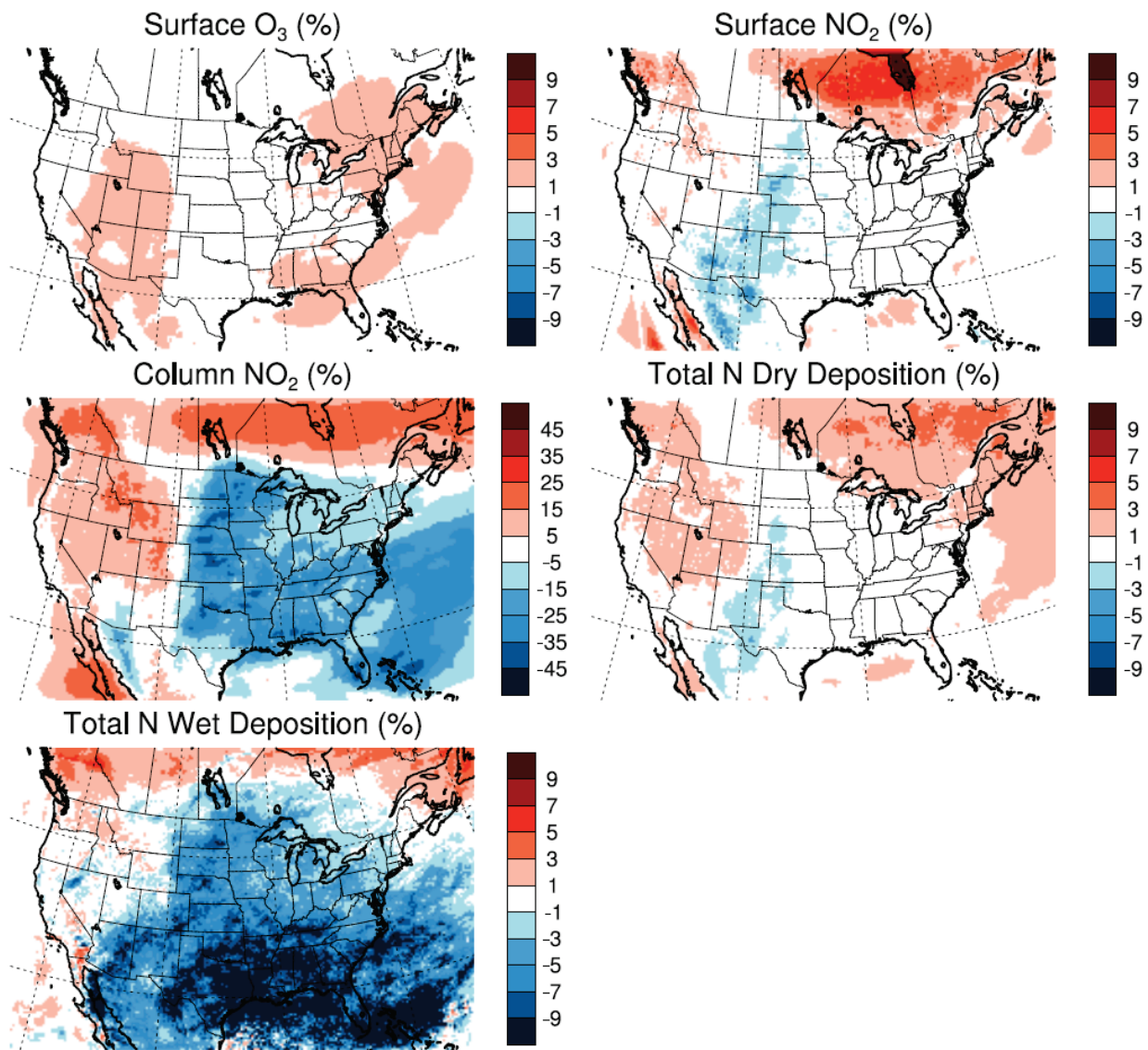
200 **Figure S4: Impact of different WRF configuration options used in this study vs. Appel et al. (2021) on annual mean surface values of several meteorological fields, O<sub>3</sub>, and aerosol species. The maps show absolute differences calculated as M3DRY\_2016 minus M3DRY\_LTNGNO\_BASE\_2016.**



205 **Figure S5: Impact of different lateral boundary conditions used in this study vs. Appel et al. (2021) on annual mean surface values of several gas phase and aerosol species. The maps show absolute differences calculated as M3DRY\_2016 minus M3DRY\_HCMAQ\_2016.**



210 **Figure S6: Impact of different anthropogenic and fire emission files used in this study vs. Appel et al. (2021) on annual mean surface values of several gas phase and aerosol species. The maps show absolute differences calculated as M3DRY\_2016 minus M3DRY\_APPEL\_EMIS\_2016. “Soil” fine aerosol concentrations are estimated from simulated crustal elements as  $2.20 \cdot \text{Al} + 2.49 \cdot \text{Si} + 1.63 \cdot \text{Ca} + 2.42 \cdot \text{Fe} + 1.94 \cdot \text{Ti}$ .**



215

Figure S7: Impact of different lightning NO emission representation on May – September surface mixing ratios of O<sub>3</sub> and NO<sub>2</sub>, column NO<sub>2</sub>, and dry and wet deposition of total nitrogen. The maps show percentage differences calculated as M3DRY\_LTNGNO\_BASE\_2016 minus M3DRY\_LTNGNO\_NLDN\_2016 relative to M3DRY\_LTNGNO\_BASE\_2016.

220

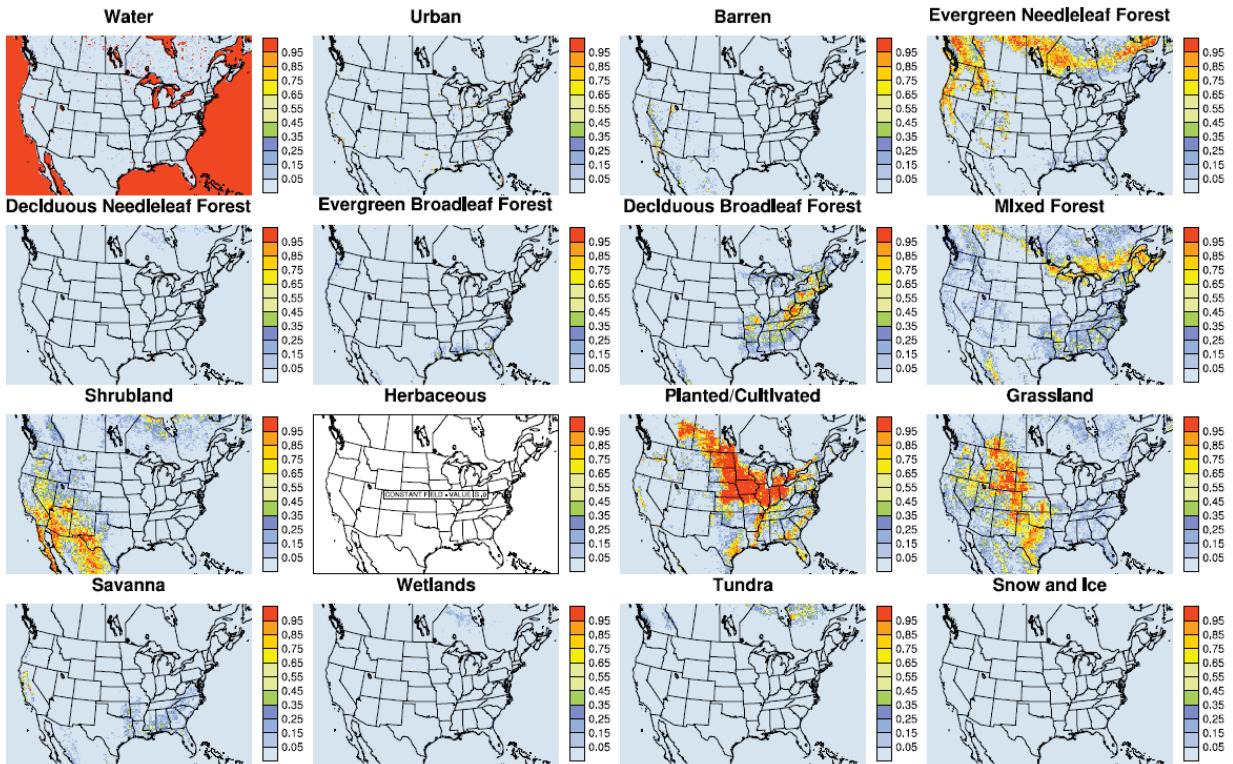
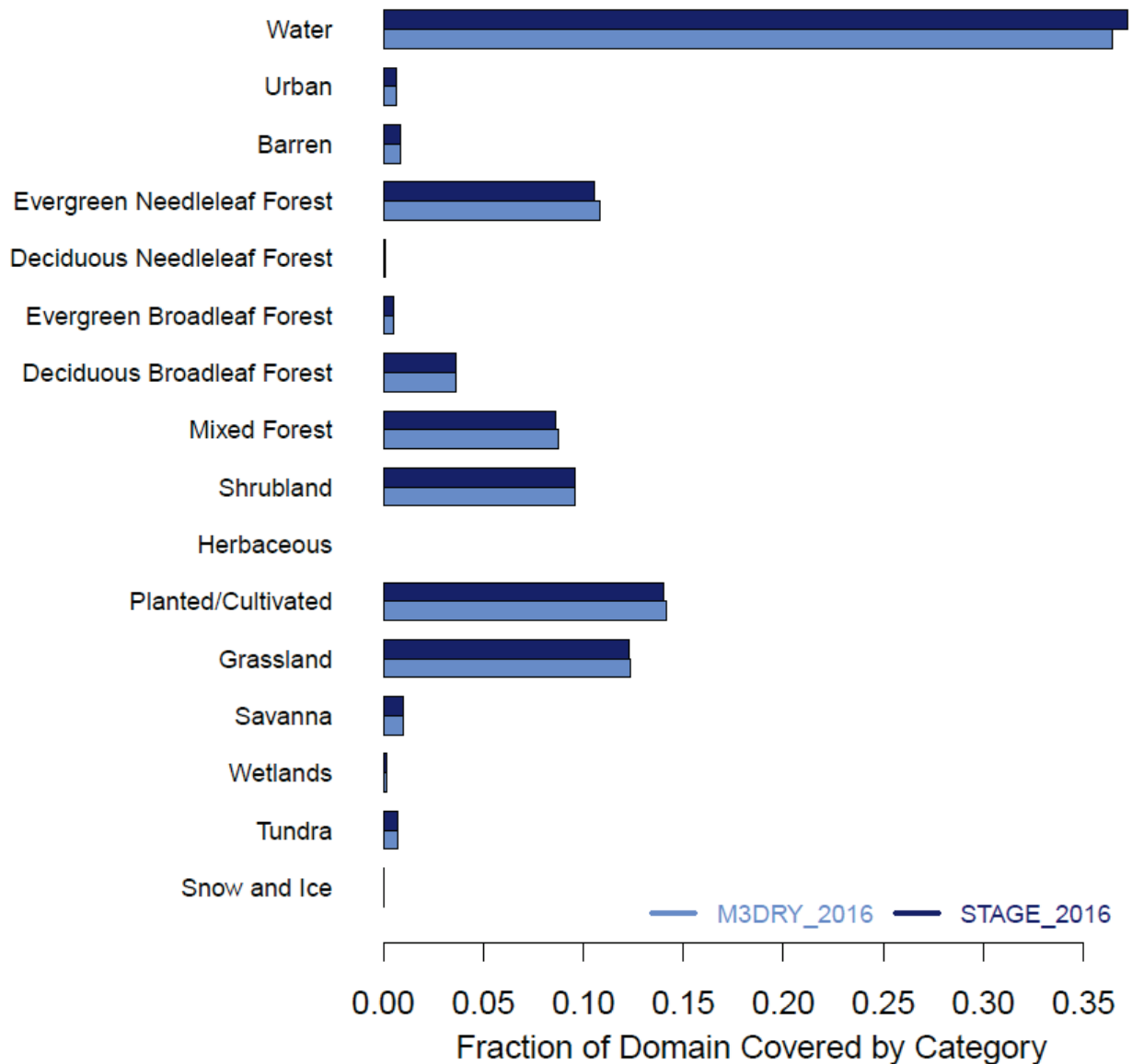


Figure S8: Maps of fractional coverage of the 16 AQMEII4 LU categories (Galmarini et al., 2021) in the M3DRY\_2016 simulations using MODIS LU. As noted in Section 2.3.1, the M3Dry simulations were performed using the 20 native MODIS LU categories and the mapping to the AQMEII4 categories was performed during post-processing. None of the 20 MODIS LU categories correspond to the AQMEII4 herbaceous category.

225



230 **Figure S9: Domainwide fractional coverage of the 16 AQMEII4 LU categories (Galmarini et al., 2021) in the**  
**M3DRY\_2016 and STAGE\_2016 simulations. As noted in Section 2.3.1, the M3Dry simulations were**  
**performed using the 20 native MODIS LU categories and the mapping to the AQMEII4 categories was**  
**performed during post-processing while the STAGE simulations were performed using the AQMEII4**  
**categories. None of the 20 MODIS LU categories correspond to the AQMEII4 herbaceous category. See**  
 235 **discussion in the text on the small differences in fractional coverage between M3DRY\_2016 and STAGE\_2016.**

$$1/R_s O_3$$

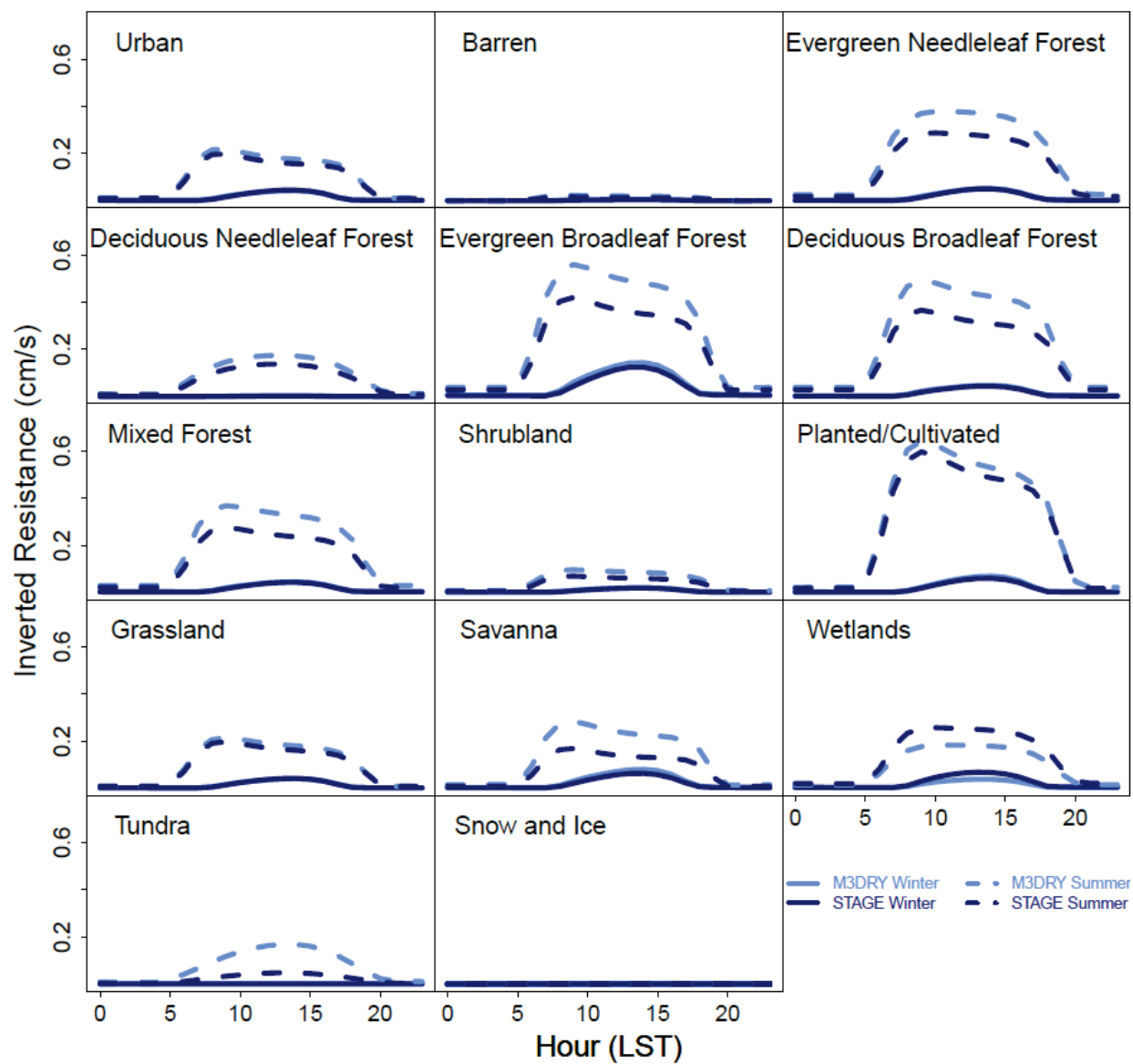
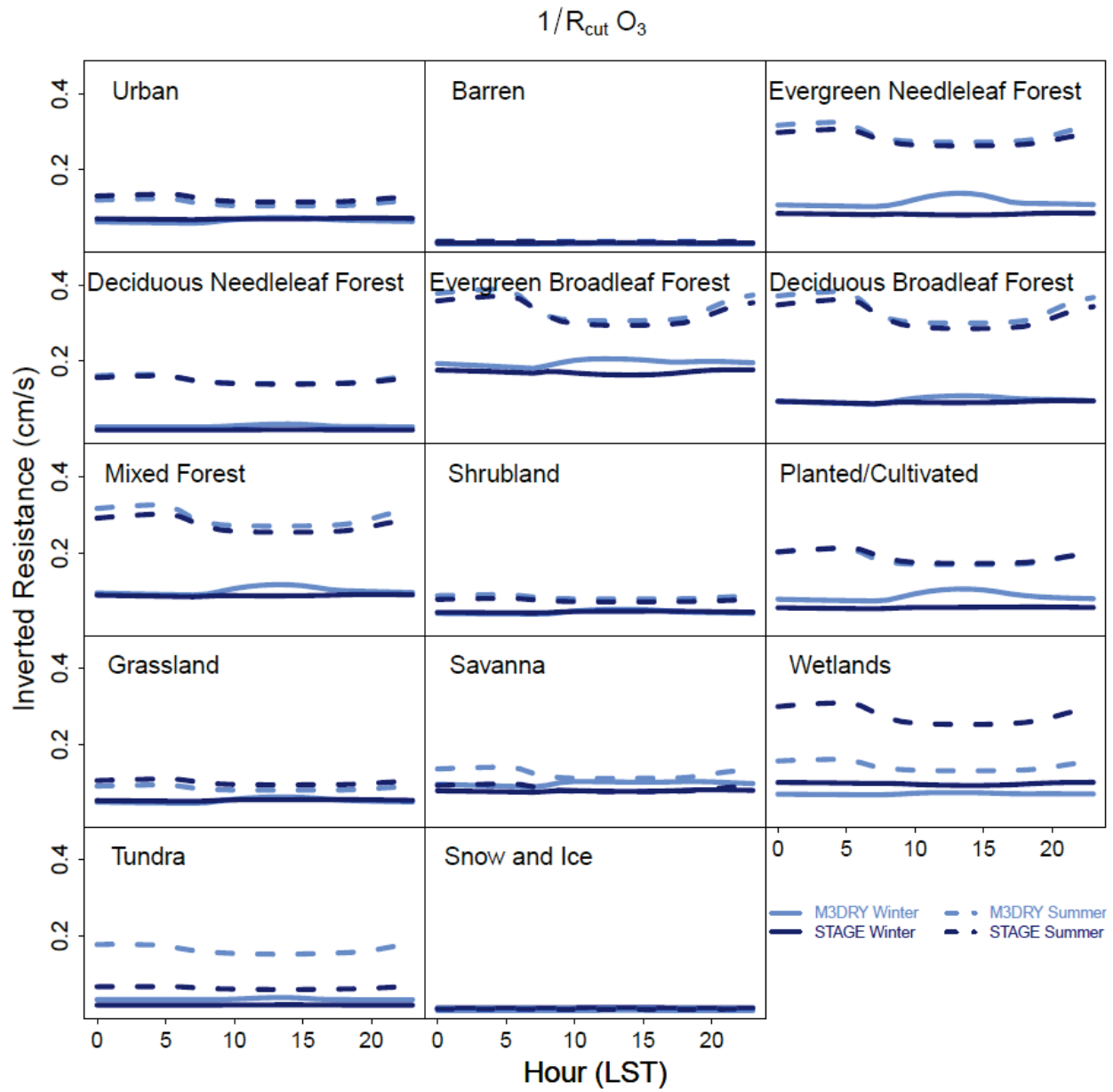
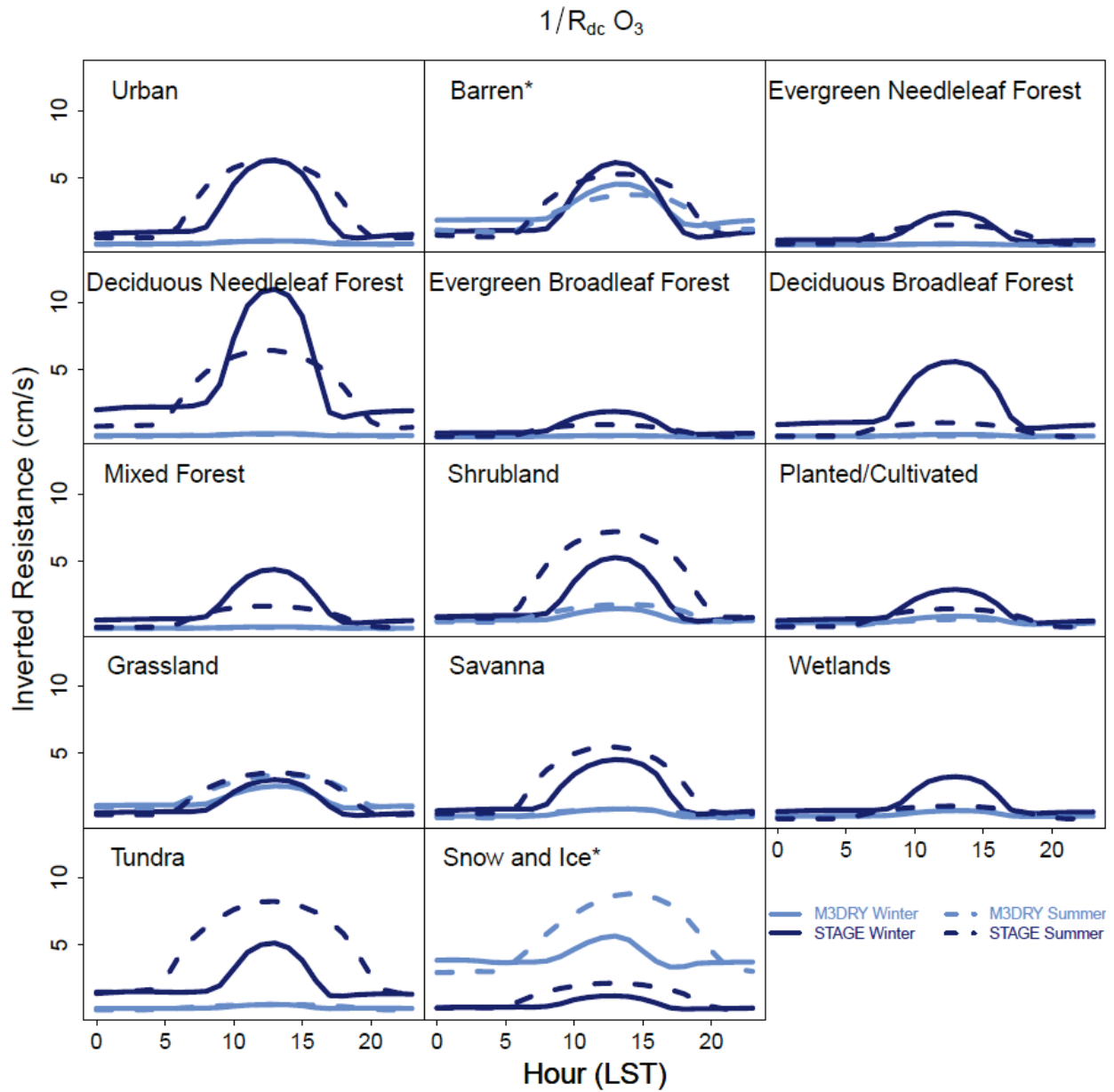


Figure S10. Domain average summer and winter diurnal cycles of LU-specific  $O_3$  inverted stomatal resistances for M3DRY\_2016 and STAGE\_2016.



240

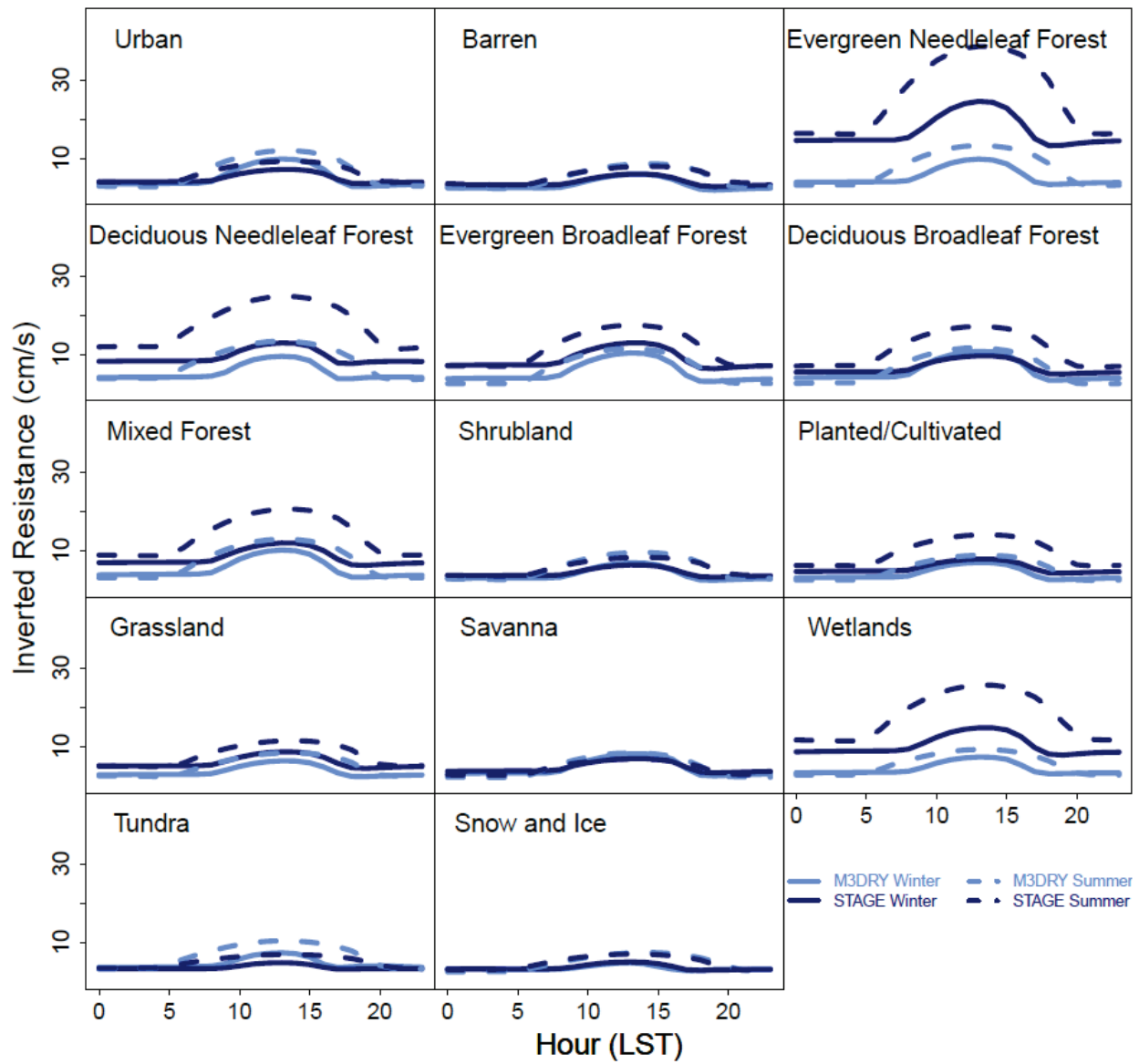
**Figure S11. Domain average summer and winter diurnal cycles of LU-specific  $\text{O}_3$  inverted cuticular resistances for M3DRY\_2016 and STAGE\_2016.**



245 **Figure S12. Domain average summer and winter diurnal cycles of LU-specific  $O_3$  inverted in-canopy convective resistances for M3DRY\_2016 and STAGE\_2016.**

\*Values for the barren and snow and ice LU categories were divided by 10 and 30, respectively, to fit on the same y-axis as values for all other LU categories

$$1/R_{\text{can,qlsb}} \text{ O}_3$$



250

Figure S13. Domain average summer and winter diurnal cycles of LU-specific  $\text{O}_3$  inverted canopy quasi-laminar sublayer resistances for M3DRY\_2016 and STAGE\_2016. Note that in M3DRY, the quasi-laminar sublayer resistance is pathway independent while in STAGE it differs between the canopy (cuticular and stomatal) and ground (vegetated and bare soil) pathways.

255

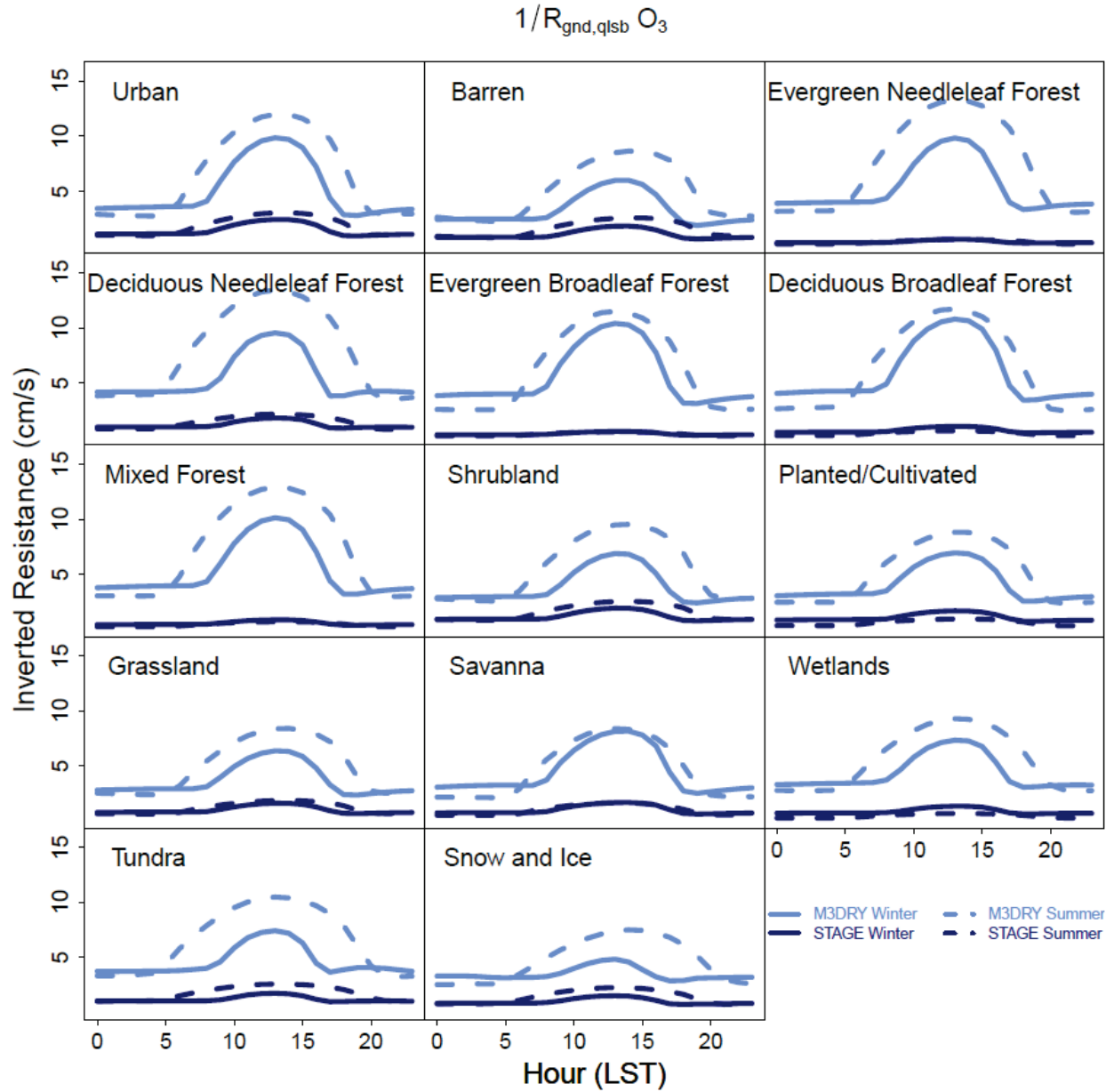
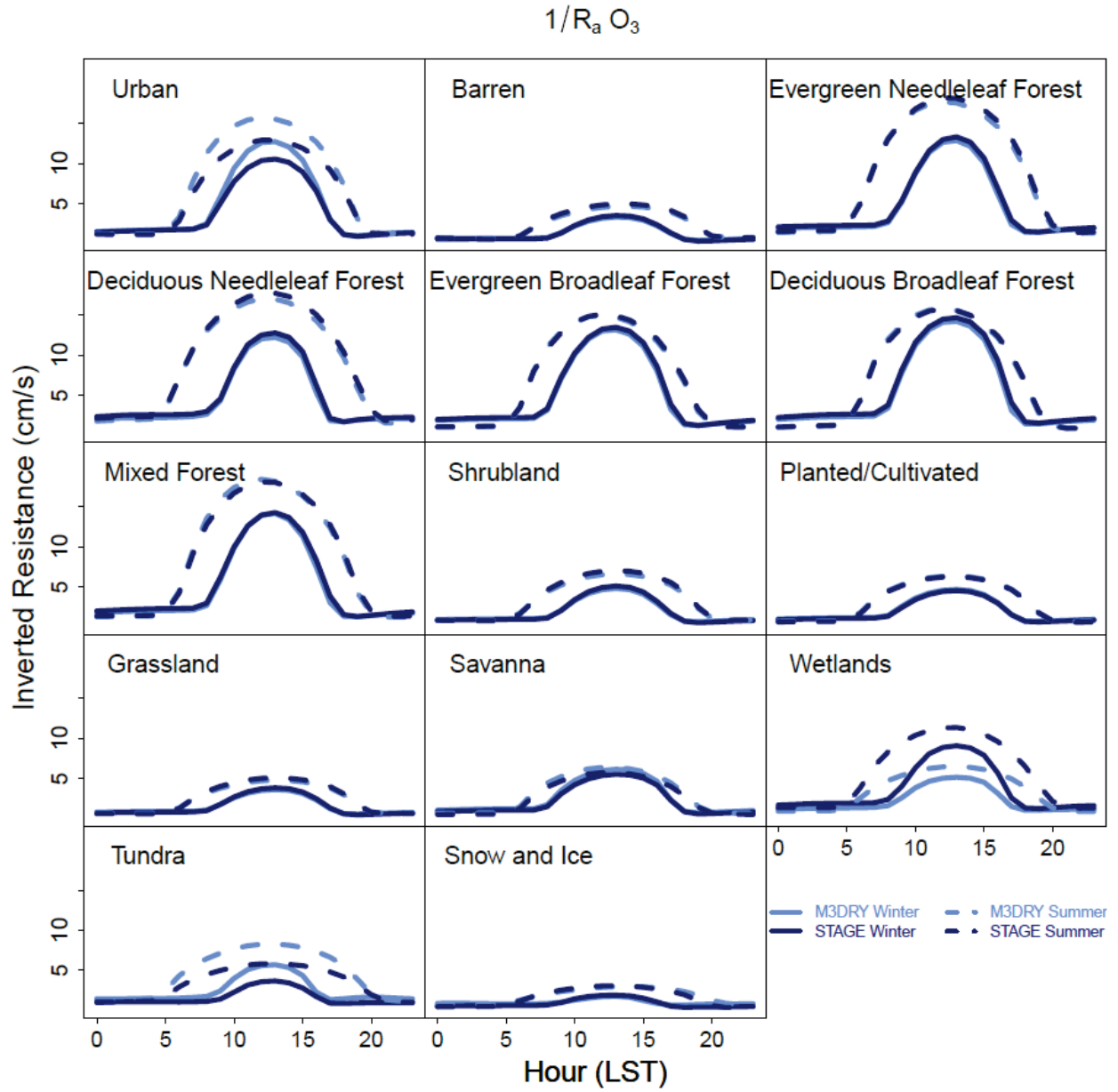


Figure S14. Domain average summer and winter diurnal cycles of LU-specific  $\text{O}_3$  inverted ground quasi-laminar sublayer resistances for M3DRY\_2016 and STAGE\_2016. Note that in M3Dry, the quasi-laminar sublayer resistance is pathway independent while in STAGE it differs between the canopy (cuticular and stomatal) and ground (vegetated and bare soil) pathways.

260



**Figure S15. Domain average summer and winter diurnal cycles of LU-specific  $O_3$  inverted aerodynamic resistances for M3DRY\_2016 and STAGE\_2016.**

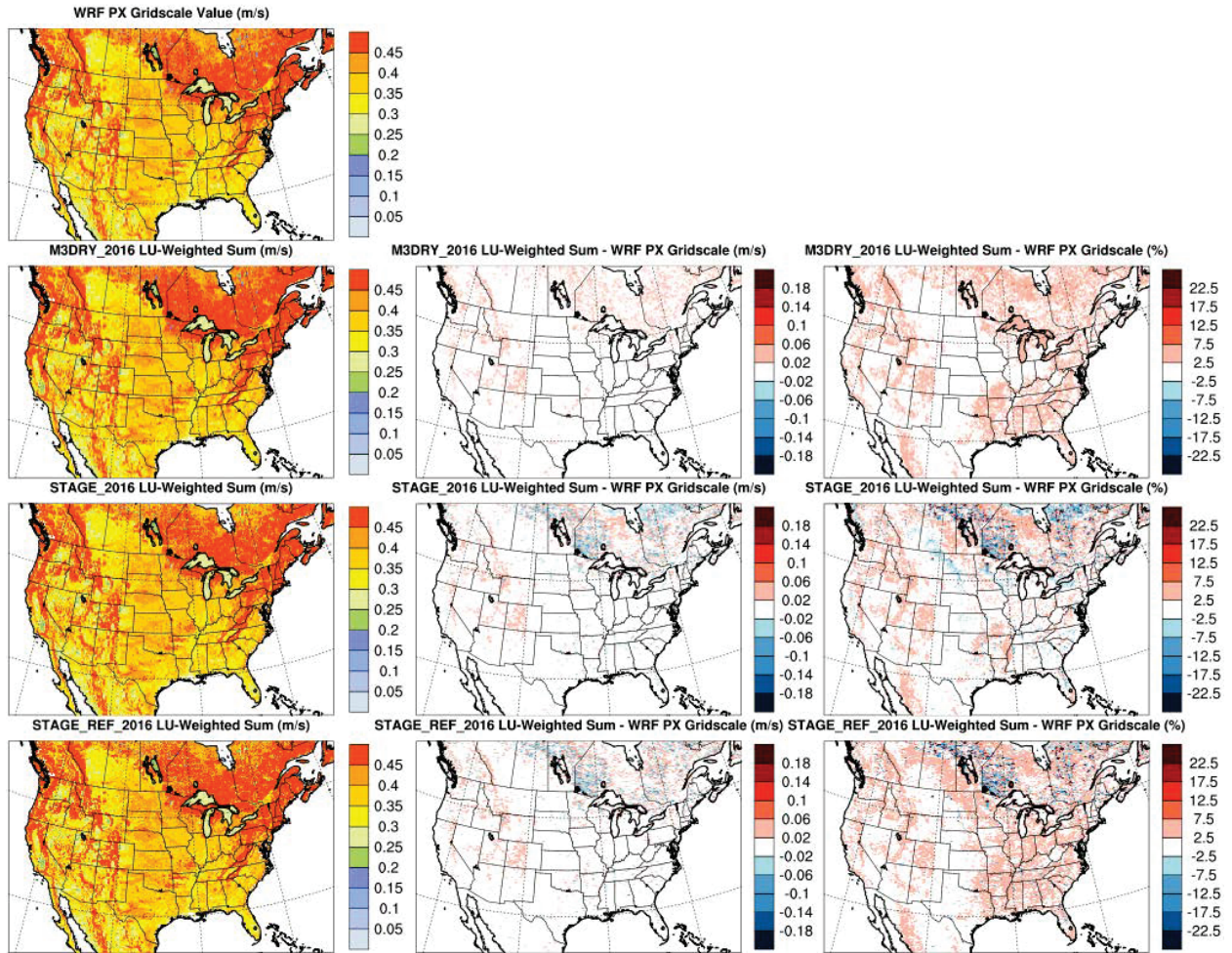
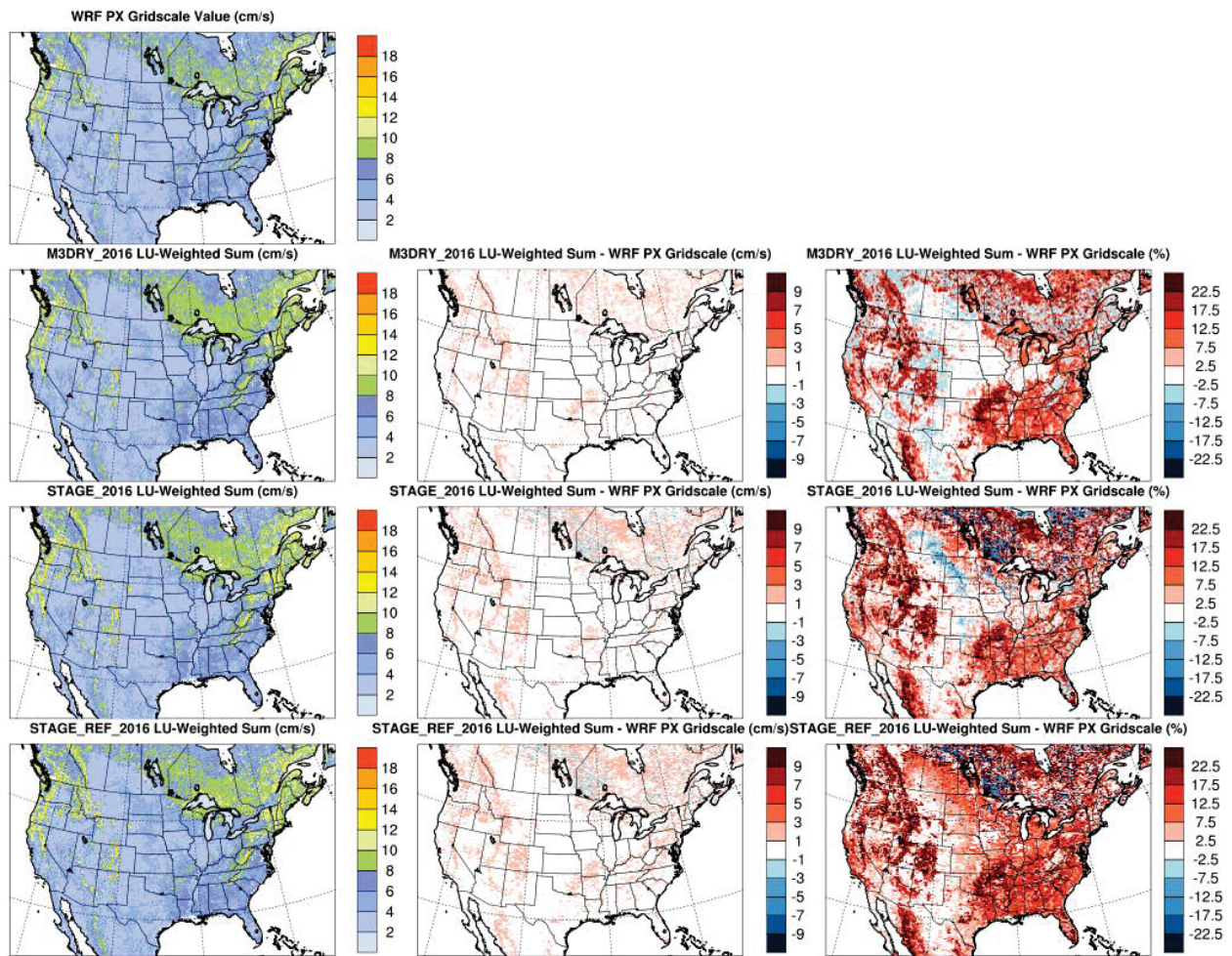
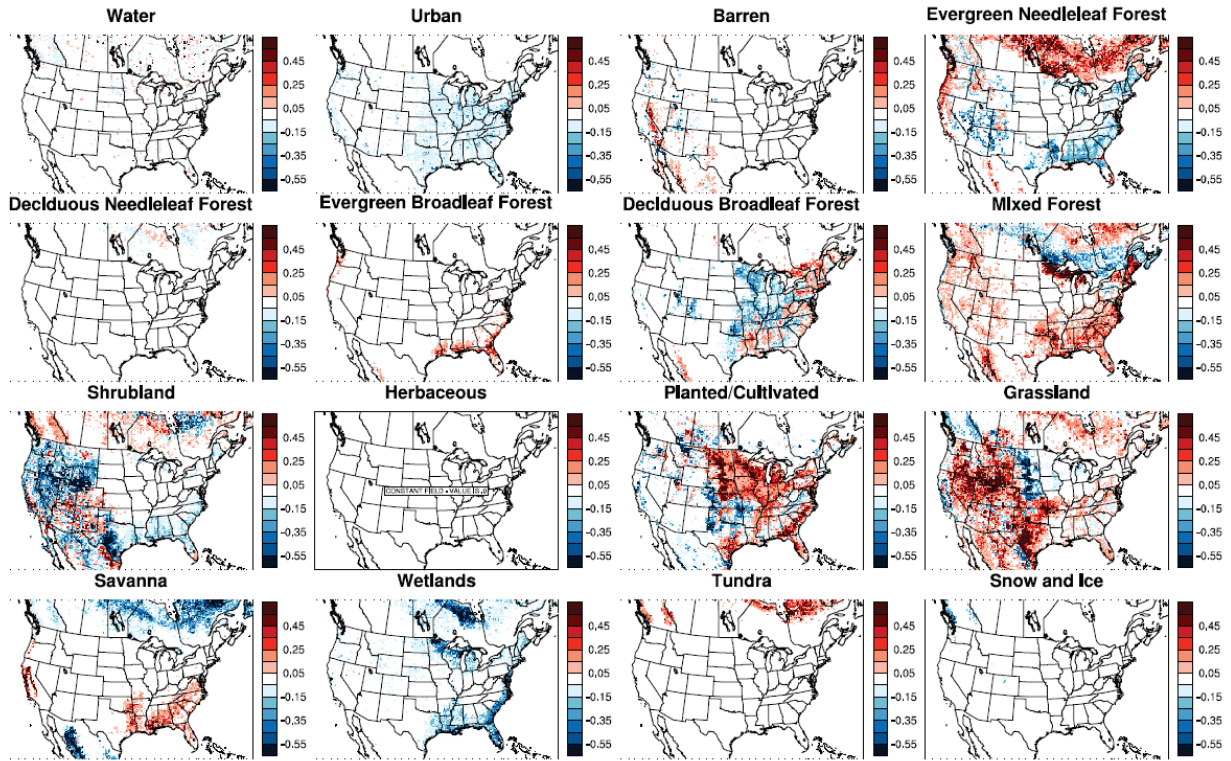


Figure S16. Left column: annual mean WRF PX grid-scale (top row) and LU-weighted sum of LU-specific  $u_*$  values for M3DRY\_2016 (second row), STAGE\_2016 (third row), and STAGE\_REF\_2016 (fourth row). Center column: absolute differences between annual mean LU-weighted sum of LU-specific and WRF PX grid-scale  $u_*$  values. Right columns: percentage differences between annual mean LU-weighted sum of LU-specific and WRF PX grid-scale  $u_*$  values.

270



275 **Figure S17. Left column: annual mean WRF PX grid-scale (top row) and LU-weighted sum of LU-specific inverted  $R_a$  values for M3DRY\_2016 (second row), STAGE\_2016 (third row), and STAGE\_REF\_2016 (fourth row). Center column: absolute differences between annual mean LU-weighted sum of LU-specific and WRF PX grid-scale inverted  $R_a$  values. Right columns: percentage differences between annual mean LU-weighted sum of LU-specific and WRF PX grid-scale inverted  $R_a$  values.**



280

Figure S18: Maps of differences in the fractional coverage of the 16 AQMEII4 LU categories (Galmarini et al., 2021) between the M3Dry simulations using WRF PX LSM configured with MODIS and NLCD LU (i.e. M3DRY\_2016 and M3DRY\_NLCD40\_2016), respectively. Differences are shown as  $M3DRY_{2016} - M3DRY_{NLCD40_{2016}}$ . As noted in Section 2.3.1, the CMAQ M3Dry calculations and post-processor estimates of LU specific and aggregated diagnostic variables were performed using native LU categories from the MODIS and NLCD schemes. Aggregation to the 16 category AQMEII4 LU scheme was performed through mapping and LU weighted averaging of equivalent categories (Table S3). None of the MODIS LU categories correspond to the AQMEII4 herbaceous category.

285

290 **References**

Appel, K. W., Bash, J. O., Fahey, K. M., Foley, K. M., Gilliam, R. C., Hogrefe, C., Hutzell, W. T., Kang, D., Mathur, R., Murphy, B. N., Napelenok, S. L., Nolte, C. G., Pleim, J. E., Pouliot, G. A., Pye, H. O. T., Ran, L., Roselle, S. J., Sarwar, G., Schwede, D. B., Sidi, F. I., Spero, T. L., and Wong, D. C.: The Community Multiscale Air Quality (CMAQ) model versions 5.3 and 5.3.1: system updates and evaluation, *Geosci. Model Dev.*, 14, 2867–2897, <https://doi.org/10.5194/gmd-14-2867-2021>, 2021

Heath, N., Pleim, J., Gilliam, R. and Kang, D.: A simple lightning assimilation technique for improving retrospective WRF simulations. *J. Adv. Model Earth Syst.*, 8, doi:10.1002/2016MS000735, 2016

Kang, D.; Hogrefe, C.; Sarwar, G.; East, J.D.; Madden, J.M.; Mathur, R.; Henderson, B.H. Assessing the Impact of Lightning NOx Emissions in CMAQ Using Lightning Flash Data from WWLLN over the Contiguous United States. *Atmosphere*, 13, 1248. <https://doi.org/10.3390/atmos13081248>, 2022

Zhang, Y., Foley, K. M., Schwede, D. B., Bash, J. O., Pinto, J. P., & Dennis, R. L.: A measurement-model fusion approach for improved wet deposition maps and trends. *Journal of Geophysical Research: Atmospheres*, 124, 4237–4251. <https://doi.org/10.1029/2018JD029051>, 2019